ACS Photonics

pubs.acs.org/journal/apchd5

Article

Dual-Polarization Analog 2D Image Processing with Nonlocal Metasurfaces

Hoyeong Kwon, Andrea Cordaro, Dimitrios Sounas, Albert Polman, and Andrea Alù*

Cite This: *ACS Photonics* 2020, 7, 1799−1805

Read Online

ACCESS | Metrics & More | Article Recommendations | Supporting Information

ABSTRACT: Optical analog computing using metasurfaces has been the subject of numerous studies, aimed at implementing highly efficient and ultrafast image processing in a compact device. The proposed approaches to date have shown limitations in terms of spatial resolution, overall efficiency, polarization and azimuthal angular dependence. Here, we present the design of a polarization-insensitive metasurface with tailored nonlocality based on a Fano resonant response, enabling both odd- and even-order analog mathematical operations on an incoming image. The metasurface is formed by a single-layered triangular lattice of holes in a suspended silicon membrane, which induces a strong nonlocal response in the transverse spatial frequency spectrum. Our paper provides a path to realize highly efficient optical metasurfaces performing isotropic and polarization-insensitive edge detection on an arbitrary 2D optical image.

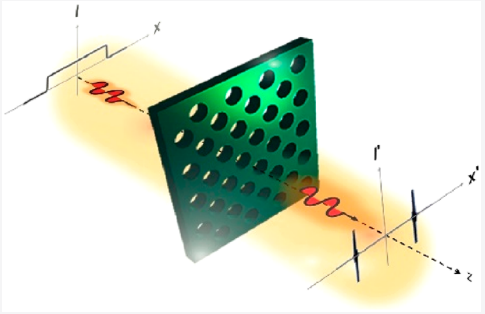

KEYWORDS: *computational metasurfaces, analog processing, nonlocality, Fano resonance, polarization-insensitive*

Implementing the functionalities of digital signal processing systems into a compact and highly efficient analog computing platform has raised significant interest in recent times.[1−15] This trend has been accelerated by the benefits that metasurfaces provide in terms of wavefront shaping, integrability with detector schemes, ultrathin footprint, and ultrafast response, overcoming the current limitations of digital processing concerning energy consumption and speed.[16−21] As a result, computational metasurfaces for optical signal processing have recently drawn significant attention and interest. So far, different approaches have been explored to perform various types of operations for image processing, for example, n^{th}-order differentiation or integration,[1−15] which can also lead to solving integro-differential equations once feedback is introduced.[22] Graded-index fibers, surface plasmon waveguides, Mach−Zehnder interferometer meshes, and metamaterials have been proposed as possible platforms for the practical implementation of these concepts, however, the proposed devices to date have presented limitations in terms of resolution, efficiency, and strong polarization/angle dependence.[23−25] In addition, the proposed optical metasurfaces have been typically limited to even-order mathematical operations, such as the second derivative.[6,7,15]

Recent works have shown that Fano resonances can be used to engineer a metasurface nonlocality and hence tailor the angular spectrum of an image to impart a linear mathematical operation of choice.[26−28] Nonlocality results in variation of the metasurface response with respect to the incident direction. By suitably engineering nonlocality in momentum space, the metasurface can be designed to exhibit various mathematical operations for a desired NA (numerical aperture). A first design based on modulated split-ring-resonator arrays[29] at microwave frequencies was introduced in ref 8, while an experimental verification in optics using one-dimensional (1D) metasurfaces composed of silicon nanobeams was presented in ref 9. These two implementations, however, were limited to a single impinging polarization and plane of incidence, serving as a proof-of-concept, but with limited impact for practical applications. Here, we show a two-dimensional (2D) metasurface that can faithfully perform even and odd mathematical operations on an impinging image independent of the polarization and incidence angles. The design is based on a triangular lattice of air holes carved into a suspended silicon membrane, which sustains a Fano resonance stemming from the coupling of a leaky-wave mode to a longitudinal Fabry−Perot resonance (see Supporting Information (SI) and refs 26−28). A similar resonant behavior can be achieved with a lattice of high-index particles.[30] The proposed metasurface offers tailored spatial frequency resolution and polarization-insensitive operation within a single layered thin metasurface, amenable for fabrication and integration into a more complex imaging system. One of the applications of this device is all-optical edge detection of an input image.[31,32] By implementing an isotropic response across all transverse momentum space, we show that the

Received: March 25, 2020
Published: June 9, 2020

https://dx.doi.org/10.1021/acsphotonics.0c00473
ACS Photonics 2020, 7, 1799−1805

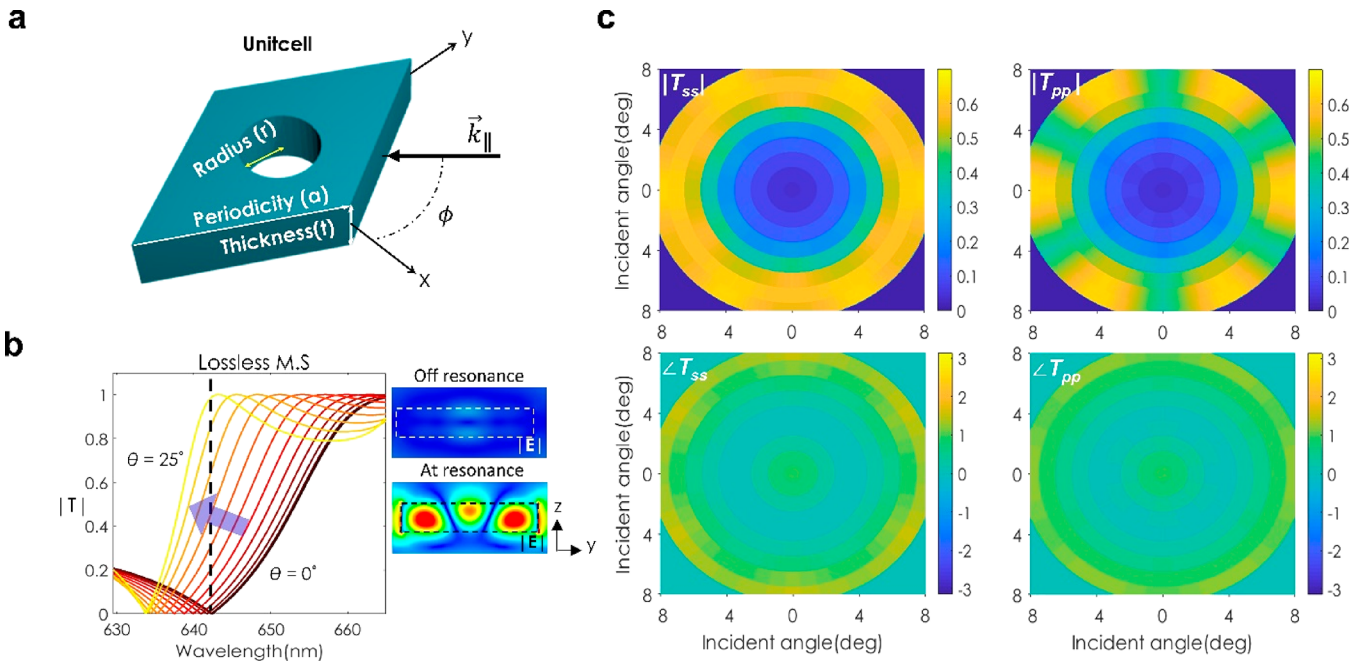

Figure 1. Metasurface for second-order differentiation. (a) Unit cell with triangular lattice and design parameters. (b) Transmission for a metasurface neglecting loss in Si for *s*-polarized light impinging at $\phi = 0°$ and different elevation angles. At resonance, the electric field is strongly enhanced compared to the off-resonance wavelength. This metasurface is designed with $a = 360$ nm, $r = 100$ nm, and $t = 125$ nm and operates at $\lambda = 643$ nm. The inset shows the time-averaged field intensity on (at $\lambda = 643$ nm) and off resonance (at $\lambda = 655$ nm). (c) 2D transmission of the optimal design including Si loss. The transmission reaches a peak of 0.7 isotropically in all transverse momentum space supported by the lattice symmetry, and the transmission phase is symmetric in all transverse propagation directions. The cross-polarized response is negligible (see SI).

metasurface can perform both even- and odd-order differentiations, enabling high-quality, efficient 2D edge detection for unpolarized input signals.

THEORETICAL ANALYSIS

Consider a linearly polarized beam impinging on our metasurface, corresponding to an arbitrary 2D image, with a transverse field profile $\boldsymbol{E}^{\text{in}}_{x,y}(x, y) = \begin{pmatrix} E^{\text{in}}_x(x, y) \\ E^{\text{in}}_y(x, y) \end{pmatrix}$, where E^{in}_x and E^{in}_y are on the x- and y-polarized field components. Upon interaction with the metasurface, the input beam is filtered in momentum space ($\mathbf{k}$-space) by the 2×2 transmission tensor $\overline{\overline{T}} = \begin{pmatrix} \tilde{T}_{ss}(k_x, k_y) & \tilde{T}_{sp}(k_x, k_y) \\ \tilde{T}_{ps}(k_x, k_y) & \tilde{T}_{pp}(k_x, k_y) \end{pmatrix}$ of the metasurface, where $\tilde{T}_{uv}$ is the transmission coefficient from an input v-polarized wave to an output u-polarized one with transverse wavevector $\mathbf{k}_{\parallel} = k_x\hat{x} + k_y\hat{y}$. Here we have assumed that our metasurface is transversely invariant, hence transverse momentum is conserved for each plane-wave component of the impinging image. The output signal is calculated as follows. The input signal is Fourier transformed into $\tilde{\boldsymbol{E}}^{\text{in}}_{x,y}(k_x, k_y)$ and converted into the *sp*-polarization basis via multiplication with $\overline{\overline{R}} = \begin{pmatrix} \sin\phi & \cos\phi \\ -\cos\phi & \sin\phi \end{pmatrix}$, where ϕ is the azimuthal angle between $\mathbf{k}_{\parallel}$ and the x-axis (see Figure 1a). This spectrum is filtered by the metasurface transfer function $\overline{\overline{T}}$ and projected back onto the xy-polarization basis by multiplying it with $\overline{\overline{R}}^{-1}$. Finally, an inverse Fourier transform is performed to derive the spatial profile of the output field. These steps are captured in the following equation for the transmitted image (see SI).

$$\begin{pmatrix} E^{\text{out}}_x(x, y) \\ E^{\text{out}}_y(x, y) \end{pmatrix} = \mathcal{F}^{-1}\left[\overline{\overline{R}}^{-1}\begin{pmatrix} \tilde{T}_{ss}(k_x, k_y) & \tilde{T}_{sp}(k_x, k_y) \\ \tilde{T}_{ps}(k_x, k_y) & \tilde{T}_{pp}(k_x, k_y) \end{pmatrix}\overline{\overline{R}}\left(\mathcal{F}\begin{bmatrix} E^{in}_x(x, y) \\ E^{in}_y(x, y) \end{bmatrix}\right)\right] \quad (1)$$

where $\mathcal{F}$ denotes the Fourier transform.

Within this formalism, the response function corresponding to an isotropic operation is defined as $\overline{\overline{T}}(k_x,k_y) = T(k_x,k_y)\mathbf{I}_{2\times2}$, where $T(k_x,k_y)$ is an arbitrary scalar function and $\mathbf{I}_{2\times2}$ is the 2×2 identity matrix. If the response is also azimuthally symmetric, $T(k_x,k_y) = T(k_{\parallel})$, where $k_{\parallel} = (k_x^2 + k_y^2)^{1/2} = k_0 \sin\theta$ and θ is the incidence angle with respect to the normal direction to the metasurface. In the case of differentiation, azimuthal symmetry is only possible for even-order operations, in which case $T_n(k_{\parallel}) = A_n(-jk_{\parallel})^n$, where n is the differentiation order and A_n is a constant. For example, in the case of second-order differentiation, the response becomes the Laplace operator $\overline{\overline{T}}_2(k_x,k_y) = -A_2(k_{\parallel})^2\mathbf{I}_{2\times2} = -A_2(k_0 \sin\theta)^2\,\mathbf{I}_{2\times2}$, where $k_0 = 2\pi/\lambda$ is the free-space wavenumber. Interestingly, as will become clearer later in the analysis, azimuthal symmetry is not possible for odd-order differentiation. For this type of operations, $T(k_x, k_y)$ can be defined along a radial direction as $T_n(k_x, k_y) = A_n(\phi)(-jk_{\parallel})^n$, where $A_n(\phi)$ is a function of the azimuthal angle ϕ. As an example, the first-order differentiation is described through $\overline{\overline{T}}_1(k_x,k_y) = -jA_1(\phi)(k_{\parallel})\mathbf{I}_{2\times2} = -jA_1(k_0 \sin\theta)\mathbf{I}_{2\times2}$ and involves a 180° phase jump with respect to $\theta = 0°$ (normal incidence). As shown in ref 8, implementing such an operation requires metasurfaces breaking symmetries in both transverse and longitudinal directions.

There are two important figures-of-merit to be considered when implementing an image processing metasurface: resolution and efficiency. In order to achieve maximum efficiency, the metasurface transmission at the highest $k_{\parallel}$ that is sought to be processed by the metasurface should reach unity. Considering realistic losses, maximum transmission for a desired

https://dx.doi.org/10.1021/acsphotonics.0c00473
ACS Photonics 2020, 7, 1799−1805

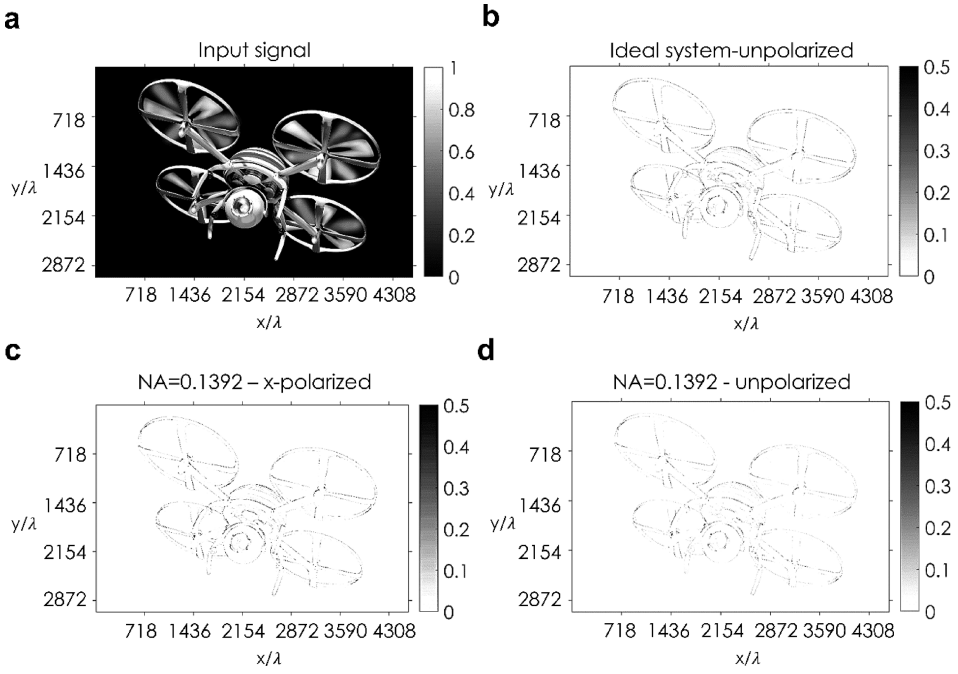

Figure 2. Second-order differentiation of a 2D image. (a) A complex 2D input image is used to test the edge detection functionality in all transverse momentum space. (b) Output after an ideal Laplacian differentiation system for an unpolarized input image (a). (c) Output after the metasurface for an *x*-polarized input image. (d) Output after the metasurface for an unpolarized input image.

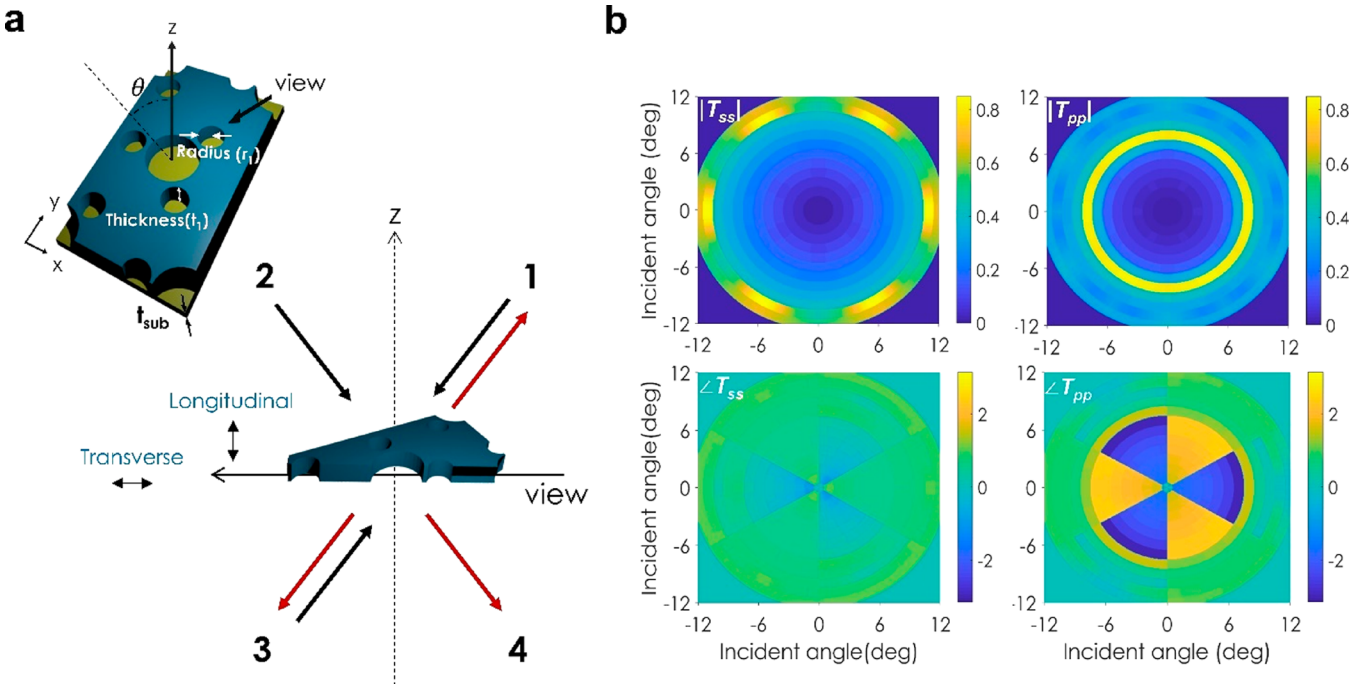

Figure 3. Metasurface for first-order differentiation. (a) Schematics of a four-port illumination of the metasurface to outline the role of symmetries in implementing odd operations. The top-left figure is a schematic view of the optimal metasurface design that performs odd-order differentiation. (b) Metasurface transmission amplitude and phase for copolarized light illumination. The amplitude of the cross-polarized system response is negligible (see SI).

maximum $k_{\parallel}$ is smaller than unity. The maximum $k_{\parallel}$ is inversely proportional to the finest size of the input image that can be processed by the metasurface and, therefore, defines its resolution.[33] In turn, a maximum $k_{\parallel}$ defines a maximum incident angle θ_{max}, which directly defines the numerical aperture (NA) of our system. It is important to stress that the possibility of tailoring the NA not only allows direct control on the resolution, but also makes our structure suitable for direct integration in detection and imaging systems. For instance, the metasurface can be directly placed on the charge-coupled device (CCD) of an existing imaging system without further optics needed. A detailed description of how to design the NA of our metasurface is provided in the SI.

https://dx.doi.org/10.1021/acsphotonics.0c00473
ACS Photonics 2020, 7, 1799−1805

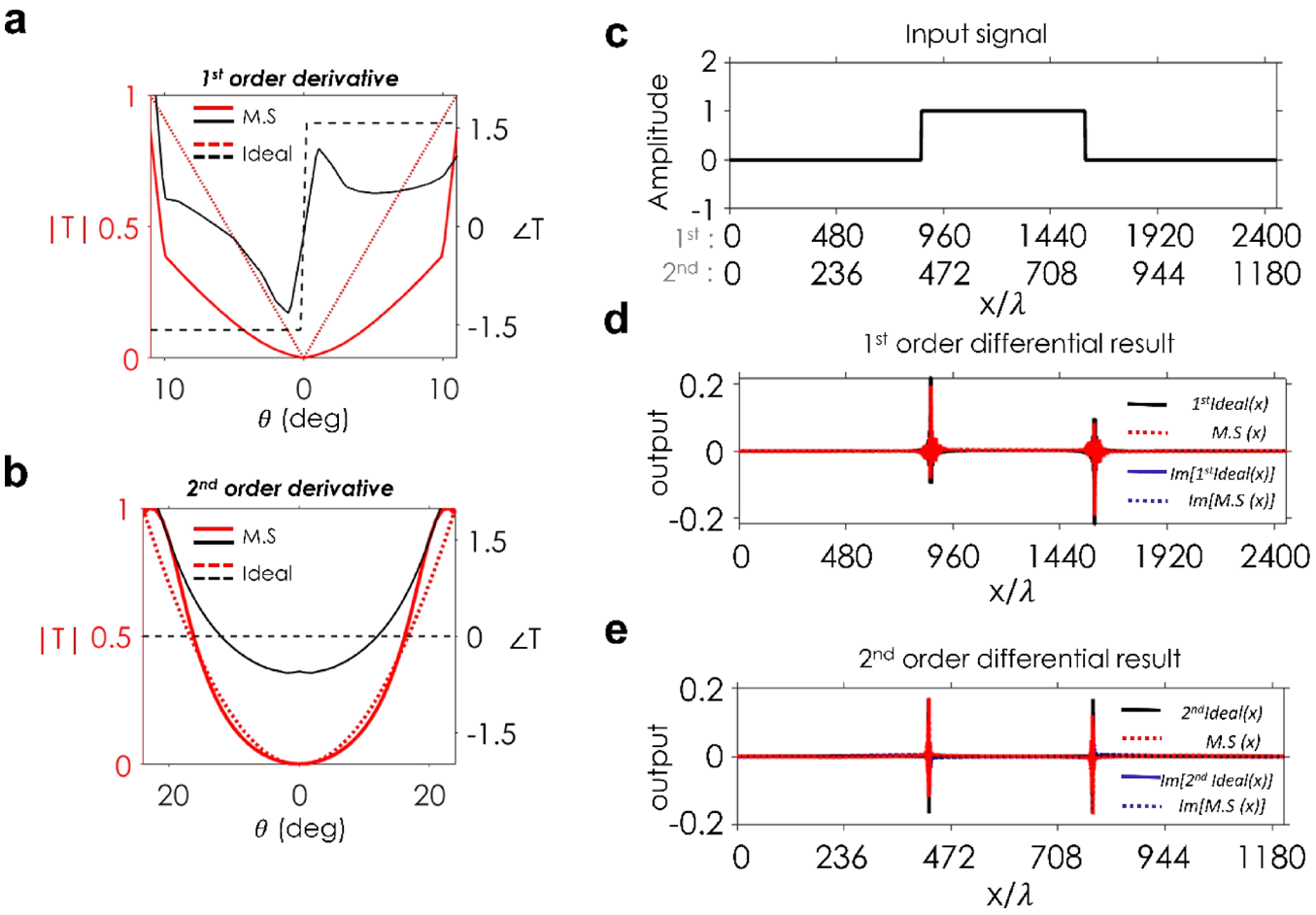

Figure 4. Comparison of 1D output for differentiating metasurfaces. (a) Transmission amplitude and phase for the first-order differential metasurface for $\phi = 0°$. (b) Response of the second-order differential metasurface at $\phi = 0°$. Both (a) and (b) are derived for *s*-polarization. (c) Amplitude profile of the 1D rectangular input signal. Here, the phase of the input signal is assumed to be zero. (d) Output after the ideal and metasurface system response in (a). (e) Output after the ideal and metasurface system response in (b).

RESULTS

In this section, we present optimized metasurface designs for first- and second-order spatial differentiations and numerically test the operation performance on 2D optical input image. The transmission spectra as a function of incoming wavelength are simulated using CST Studio Suite 2018,[34] while COMSOL Multiphysics 5.4 is used to compute the transmission for different angles of incidence at the designed wavelength of operation.[35] The predicted image output is obtained using eq 1.

Our second-order differential metasurface consists of a triangular array of air holes (lattice constant a and radius r) carved in a thin Si membrane of thickness t, as shown in Figure 1a. Such a structure supports Fano resonances obtained through the interference of a broad Fabry−Perot resonance determined by the thickness and fill fraction of the metasurface and leaky wave resonances, which are essentially guided waves that are coupled to the radiation continuum through the periodic hole grating (see SI). As a result, the leaky wave resonance and consequently the Fano resonance follow the same dispersion as the guided mode in terms of frequency versus transverse wavenumber $k_{\|} = k_0 \sin \theta$. The transmission dispersion in transverse momentum space is determined by the resonance frequency of this surface wave as $\vec{k}_{\|} + \vec{k}_r$, where $\vec{k}_r$ is a reciprocal lattice vector. Therefore, the Fano resonance exhibits strong nonlocality, manifested in a shift of the Fano resonance wavelength versus incidence angle, as shown in Figure 1b. The second-order differential operation can be achieved if the metasurface is designed to exhibit a transmission zero at normal incidence at the operation wavelength. Then, as the incidence angle increases, transmission increases, up to an angle for which transmission is maximum (see dashed line in Figure 1b). The angle of maximum transmission determines the NA of the metasurface or the maximum transverse wavenumber of the input image, as was discussed in the previous section. Given the lattice symmetry in the transverse (xy) plane, the metasurface offers a quasi-isotropic response in ϕ over the entire transverse momentum space.

The optimal metasurface parameters for second-order spatial differentiation at $\lambda = 717$ nm are $a = 250$ nm, $r = 120$ nm, and $t = 125$ nm. In Figure 1c, the top and bottom panels show the transmission amplitude and phase for the copolarized components of the transmission matrix. Cross-polarized transmission amplitudes are negligible, as shown in the SI. The design and simulations consider realistic material loss,[36] which limits the maximum achievable transmission to 0.7. Both amplitude and phase responses are symmetric in all transverse directions, as required for ideal even-order differential operation. From the amplitude profile, we can see that the metasurface supports an angular bandwidth of 8° for both *s*- and *p*-polarized illuminations, hence, allowing efficient 2D edge detection with NA = 0.1392. As mentioned before, different NAs can be

https://dx.doi.org/10.1021/acsphotonics.0c00473
ACS Photonics 2020, 7, 1799−1805

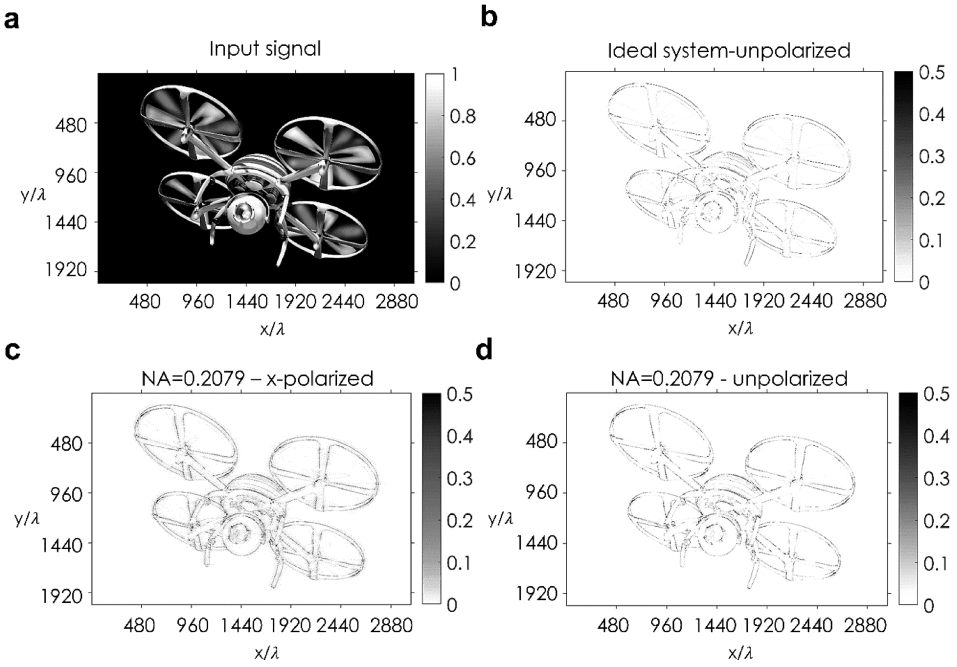

Figure 5. First-order differentiation on 2D image. (a) The same complex 2D input image as the one in Figure 2a. (b) The 2D output image after the ideal system for the unpolarized input image. The NA is set to be same as the one of the metasurface. (c) The output after the metasurface when the *x*-polarized input image is projected to the metasurface. (d) The output after the metasurface when the unpolarized input image is projected to the metasurface.

achieved by tuning the design parameters. This possibility is discussed in more detail in the SI.

In order to highlight the functionality of the metasurface, the 2D input image in Figure 2a is projected to the metasurface and the output is calculated through eq 1. The results are shown in Figure 2b–d. Figure 2b shows the ideal output from a second-order (Laplacian) operation, while Figure 2c and d refer to outputs along *x* and unpolarized light. The *x*- and *y*-axes in these figures are normalized to the operation wavelength, and the color refers to the intensity scale. The metasurface detects edges in all transverse directions with high efficiency for linear and unpolarized light incidence, as shown in Figure 2c,d. Overall, the metasurface response is very close to the one of the ideal system in Figure 2b. Since the metasurface exhibits the same resolution for both polarizations, it can perform edge detection for any polarization and even unpolarized light. An analysis of this case is presented in the SI.

In order to implement odd-order differentiation, the transmission phase needs to be an odd function of the incidence angle, which requires breaking both transverse and longitudinal symmetries in the metasurface.[8] This fact can be understood through Figure 3a. If the structure were symmetric with respect to the *z*-axis, $T_{42} = T_{13}$. However, reciprocity also requires $T_{31} = T_{13}$, leading to $T_{42} = T_{31}$, which shows that transmission is an even function versus the incidence angle. Therefore, in order to achieve an odd response, we need to break both transverse and longitudinal mirror symmetries. To this end, our unit cell is modified as shown in the inset of Figure 3a, adding a thin SiO_2 substrate to break longitudinal symmetry (the symmetry parallel to the *z* axis) and three small holes symmetrically distributed around the main hole to break transverse symmetry (the symmetry on the *xy*-plane). The transmission for copolarized fields is shown in Figure 3b. As mentioned in the previous section, the metasurface exhibits an odd-order response along any radial direction, but it lacks rotational symmetry as in even-order differentiation. The metasurface achieves a near-π phase jump between the negative and positive transverse propagation momentum, which enables the first-order differential operation at $\lambda = 628$ nm. Cross-polarized transmission is again negligible (see SI) and the metasurface performs differentiation with a NA of 0.2079 and 0.1392 for *s*- and *p*-polarizations, respectively. The metasurface design parameters are $a = 300$ nm, $r = 130$ nm, $r_1 = 77$ nm, $t = 130$ nm, $t_1 = 90$ nm, $t_{sub} = 50$ nm, and we assume the material is lossless in this calculation, considering only the real part of dispersive refractive index *n*.

To compare the response for first- and second-order differential metasurfaces, the transmission for *s*-polarization at $\phi = 0°$ is shown in Figure 4a,b for the metasurfaces in Figure 1c,b. We test the response for a 1D slit image in Figure 4c (the signal in Figure 4c is assumed to be uniform along the *y*-axis), and the outputs are shown in Figure 4d,e. As expected, the first-order differential metasurface shows a single spike with opposite signs at upward and downward edges, whereas the output of the second-order differential metasurface yields two spikes at each edge, which indicates that the first-order differentiator supports more precise and accurate edge detection than the second-order differentiator (see SI). Next, we explore the effect of the first-order differential metasurface on the 2D input image in Figure 5a for different polarizations. Analogous to the output image for an ideal first derivative (Figure 5b), the output after the metasurface shows clear edge detection in all directions, highlighting all boundaries of the object both for *x*-polarized and unpolarized illuminations, even with a small difference of NAs between *s*- and *p*-polarizations. Differences on 2D edge detection between the first- and the second-order differentiators are compared and provided in more detail in the SI, showing that the first-order differentiator is more optimal for the purpose of precise edge detection applications than the second-order differentiator.

https://dx.doi.org/10.1021/acsphotonics.0c00473
ACS Photonics 2020, 7, 1799–1805

CONCLUSIONS

In this paper, we have presented the design of 2D nonlocal metasurfaces composed of suspended Si and SiO_2, which can perform polarization independent, isotropic 2D optical image processing. The metasurface can be engineered to perform even and odd differential operations with high spatial frequency resolution and efficiency. Different types of mathematical operations, for example, the integral operation for blurring can be realized by engineering the nonlocal response in such a way to align a peak, rather than a zero, of the Fano response at the frequency of operation (see SI). By adding a form of feedback and studying the steady-state response of the system, it is possible to implement also integro-differential equation solvers based on a similar platform. Our study shows realistic pathways to implement analog optical processing of large images with an ultrathin metasurface at visible frequencies, directly integrable on optical sensors, with applications in the design of ultrafast and power-efficient optical processing systems.

ASSOCIATED CONTENT

Supporting Information

The Supporting Information is available free of charge at https://pubs.acs.org/doi/10.1021/acsphotonics.0c00473.

> Here, we provide the theoretical and simulated data of Fano response and its nonlocality, and show that these metasurfaces can perform the 2D mathematical operations. We explain how the 2D optical input image is projected to the metasurface of a certain transfer function, and provide the steps to calculate the output after the metasurface. Then, the way to engineer the nonlocal response in space is addressed to control the numerical aperture of the operation by modifying the geometry of the metasurfaces. Finally, the difference between odd and even order differential operations are provided with the simulated results, and the way to design the metasurface that performs the passive integral operation is provided at the end (PDF)

AUTHOR INFORMATION

Corresponding Author

Andrea Alù − *Department of Electrical and Computer Engineering, The University of Texas at Austin, Austin, Texas, United States; Photonics Initiative, Advanced Science Research Center and Physics Program, Graduate Center, City University of New York, New York, New York, United States;* orcid.org/0000-0002-4297-5274; Email: alu@mail.utexas.edu

Authors

Hoyeong Kwon − *Department of Electrical and Computer Engineering, The University of Texas at Austin, Austin, Texas, United States*

Andrea Cordaro − *Van der Waals-Zeeman Institute, Institute of Physics, University of Amsterdam, 1098 XH Amsterdam, The Netherlands; Center for Nanophotonics, AMOLF, 1098 XG Amsterdam, The Netherlands;* orcid.org/0000-0003-3000-7943

Dimitrios Sounas − *Department of Electrical and Computer Engineering, Wayne State University, Detroit, Michigan, United States*

Albert Polman − *Center for Nanophotonics, AMOLF, 1098 XG Amsterdam, The Netherlands;* orcid.org/0000-0002-0685-3886

Complete contact information is available at: https://pubs.acs.org/10.1021/acsphotonics.0c00473

Notes

The authors declare no competing financial interest.

ACKNOWLEDGMENTS

This work was supported by the Air Force Office of Scientific Research MURI with Grant No. FA9550-17-1-0002. Work at AMOLF was partly financed by the Dutch Research Council (NWO).

REFERENCES

(1) Silva, A.; Monticone, F.; Castaldi, G.; Galdi, V.; Alù, A.; Engheta, N. Performing Mathematical Operations with Metamaterials. *Science* **2014**, *343*, 160−163.

(2) Solli, D. R.; Jalali, B. Analog optical computing. *Nat. Photonics* **2015**, *9*, 704−706.

(3) Pors, A.; Nielsen, M. G.; Bozhevolnyi, S. I. Analog Computing Using Reflective Plasmonic Metasurfaces. *Nano Lett.* **2015**, *15*, 791−797.

(4) Youssefi, A.; Zangeneh-Nejad, F.; Abdollahramezani, S.; Khavasi, A. Analog computing by Brewster effect. *Opt. Lett.* **2016**, *41*, 3467−3470.

(5) Chen, H.; An, D.; Li, Z.; Zhao, X. Performing differential operation with a silver dendritic metasurface at visible wavelengths. *Opt. Express* **2017**, *25*, 26417−26426.

(6) Guo, C.; Xiao, M.; Minkov, M.; Shi, Y.; Fan, S. A Photonic Crystal Slab Laplace operator for image differentiation. *Optica* **2018**, *5*, 251−256.

(7) Guo, C.; Xiao, M.; Minkov, M.; Shi, Y.; Fan, S. Isotropic wavevector domain image filters by a photonic crystal slab device. *J. Opt. Soc. Am. A* **2018**, *35*, 1685−1691.

(8) Kwon, H.; Sounas, D.; Cordaro, A.; Polman, A.; Alù, A. Nonlocal Metasurface for Optical Signal Processing. *Phys. Rev. Lett.* **2018**, *121*, 173004.

(9) Cordaro, A.; Kwon, H.; Sounas, D.; Koenderink, F.; Polman, A.; Alù, A. High-index dielectric metasurfaces performing mathematical operations. *Nano Lett.* **2019**, *19*, 8418−8423.

(10) Zhu, T.; Lou, Y.; Zhou, Y.; Zhang, J.; Huang, J.; Li, Y.; Luo, H.; Wen, S.; Zhu, S.; Gong, Q.; Qiu, M.; Ruan, Z. Generalized spatial differentiation from the spin Hall effect of light and its application in image processing of edge detection. *Phys. Rev. Appl.* **2019**, *11*, 034043.

(11) Momeni, A.; Rajabalipanah, H.; Abdolali, A.; Achouri, K. Generalized Optical Signal Processing Based on Multioperator Metasurfaces Synthesized by Susceptibility Tensors. *Phys. Rev. Appl.* **2019**, *11*, 064042.

(12) Davis, T. J.; Eftekhari, F.; Gómez, D. E.; Roberts, A. Metasurfaces with Asymmetric Optical Transfer Functions for Optical Signal Processing. *Phys. Rev. Lett.* **2019**, *123*, 031901.

(13) Estakhri, N. M.; Edwards, B.; Engheta, N. Inverse-designed metastructures that solve equations. *Science* **2019**, *363*, 1333.

(14) Babashah, H.; Kavehvash, Z.; Koohi, S.; Khavasi, A. Integration in analog optical computing using metasurfaces revisited: toward ideal optical integration. *J. Opt. Soc. Am. B* **2017**, *B34*, 1270−1279.

(15) Zhou, Y.; Zheng, H.; Kravchenko, I. I.; Valentine, J. Flat optics for image differentiation. *Nat. Photonics* **2020**, *14*, 316.

(16) Yu, N.; Capasso, F. Flat optics with designer metasurfaces. *Nat. Mater.* **2014**, *13*, 139−150.

(17) Kildishev, A. V.; Boltasseva, A.; Shalaev, V. M. Planar photonics with metasurfaces. *Science* **2013**, *339*, 1232009.

(18) Monticone, F.; Estakhri, N. M.; Alù, A. Full control of nanoscale optical transmission with a composite metascreen. *Phys. Rev. Lett.* **2013**, *110*, 203903.

(19) Esfandyarpour, M.; Garnett, E. C.; Cui, Y.; McGehee, M. D.; Brongersma, M. L. Metamaterial mirrors in optoelectronic devices. *Nat. Nanotechnol.* **2014**, *9*, 542−547.

(20) Kim, M.; Wong, A. M. H.; Eleftheriades, G. V. Optical Huygens metasurfaces with independent control of the magnitude and phase of the local reflection coefficients. *Phys. Rev. X* **2014**, *4*, 041042.
(21) Tretyakov, S. A. Metasurfaces for general transformations of electromagnetic fields. *Philos. Trans. R. Soc., A* **2015**, *373*, 20140362.
(22) Abdollahramezani, S.; Chizari, A.; Dorche, A. E.; Jamali, M. V.; Salehi, J. A. Dielectric metasurfaces solve differential and integro-differential equations. *Opt. Lett.* **2017**, *42*, 1197−1200.
(23) Zhu, T.; Zhou, Y.; Lou, Y.; Ye, H.; Qiu, M.; Ruan, Z.; Fan, S. Plasmonic computing of spatial differentiation. *Nat. Commun.* **2017**, *8*, 15391.
(24) Yang, J.; Ghimire, I.; Wu, P. C.; Gurung, S.; Arndt, C.; Tsai, D. P.; Lee, H. W. H. Photonic crystal fiber metalens enabled by geometric phase optical metasurfaces. *Frontiers in Optics/Laser Science* **2018**, FW6B.2.
(25) Miller, D. A. B. Perfect optics with imperfect components. *Optica* **2015**, *2*, 747−750.
(26) Chen, L.; Qiang, Z.; Yang, H.; Pang, H.; Ma, Z.; Zhou, W. Polarization and angular dependent transmissions on transferred nanomembrane Fano filters. *Opt. Express* **2009**, *17*, 8396−8406.
(27) Miroshnichenko, A. E.; Flach, S.; Kivshar, Y. S. Fano resonances in nonascale structure. *Rev. Mod. Phys.* **2010**, *82*, 2257.
(28) Limonov, M. F.; Rybin, M.V.; Poddubny, A. N.; Kivshar, Y. S. Fano resonances in photonics. *Nat. Photonics* **2017**, *11*, 543−554.
(29) Hadad, Y.; Sounas, D. L.; Alu, A. Space-time gradient metasurfaces. *Phys. Rev. B: Condens. Matter Mater. Phys.* **2015**, *92*, 100304.
(30) Born, M.; Wolf, E. *Principles of Optics*; Cambridge University Press: Cambridge, 1999.
(31) Canny, J. A computational approach to edge detection. *IEEE Trans Pattern Anal Mach Intel.* **1986**, *8*, 679−698.
(32) Marr, D.; Hildreth, E. Theory of edge detection. *Proc. R. Soc. London B* **1980**, *207*, 187−217.
(33) Chu, E. *Discrete and Continuous Fourier Transforms: Analysis, Applications and Fast Algorithms*; CRC Press: Boca Raton, FL, 2008.
(34) CST Suite Studio 2018. www.cst.com/2018. Dassault Systemes, MA, U.S.A.
(35) COMSOL Multiphysics v. 5.4., www.comsol.com. COMSOL AB, Stockholm, Sweden.
(36) Palik, E. D. *Handbook of Optical Constants of Solids*; Academic Press: San Diego, CA, 1998.

https://dx.doi.org/10.1021/acsphotonics.0c00473
ACS Photonics 2020, 7, 1799−1805